Nanoscience and Nanotechnology Research, 2017, Vol. 4, No. 3, 106-114
Available online at http://pubs.sciepub.com/nnr/4/3/4

DOI:10.12691/nnr-4-3-4

Nanocrystalline Cellulose: Synthesis from Pruning Waste of *Zizyphus spina christi* and Characterization

Sherif S. Z. Hindi*

Department of Arid Land Agriculture, Faculty of Meteorology, Environment and Arid Land Agriculture,
King Abdullaziz University, P.O. Box 80208, Jeddah 21589, Saudi Arabia
*Corresponding author: shindig@kau.edu.sa

Abstract Nanocrystalline cellulose (NCCs) was synthesized from pruning waste of *Zizyphus spina christi* using H_2SO_4 (64 %, wt/wt) under suitable hydrolysis conditions. The crystal growth of the NCCs from nano- into identical micrometric-scaled needles confirmed their ability to self-assembly. The aspect ratio of the NCCs was estimated using optical microscopy for needles, and by scanning electron microscopy (SEM) for powder, while their crystallinity index (CI), crystallite size (CS) and lattice spacing (LS) were estimated by X-ray diffraction (XRD). Thermogravimetric analysis (TGA) and differential thermal analysis (DTA) were also performed. The XRD-diffractogram of the NCCs was similar to that known for cellulose I. The CI of the NCCs was much higher (86.75%) than that for cellulose I. The CS of the NCCs was 2.78 nm that is smaller than that for cellulose I. The distance between the strata within the NCCs (LS) was found to be 0.214 nm. The TGA indicated a gradual increase in the mass loss upon heating the NCCs from 25°C up to 500°C in a flowing N_2-atmosphere. The DTA showed presence of an endothermic peak (due to H_2O-evaporation) and one exothermic peak (due to depolymerization and decomposition of the NCCs. Based on the results, the Zizyphus wood is suitable precursor for the NCCs production.

Keywords: *acid hydrolysis, nanocrystalline cellulose, aspect ratio, SEM, XRD, TGA, DTA*

Cite This Article: Sherif S. Z. Hindi, "Nanocrystalline Cellulose: Synthesis from Pruning Waste of *Zizyphus spina christi* and Characterization." *Nanoscience and Nanotechnology Research*, vol. 4, no. 3 (2017): 106-114. doi: 10.12691/nnr-4-3-4.

1. Introduction

Cellulose is the most abundant biopolymer on the Earth. By dissolving amorphous regions of microfibrils, the crystalline components were released. Colloidal NCCs rods having high aspect ratio have been attracting wide acceptance in global markets due to their unique mechanical properties, chirality, sustainability, and availability [1].

NCCs production is a depolymerization process of cellulosic fibers into a value-added nanomaterial, or producing useful chemicals and fuels [2]. In relation to the hydrolyzing agent, the NCCs were synthesized by using H_2SO_4 [3], HCl [4], HBr [5]. In addition, phosphotungstic acid ($H_3PW_{12}O_{40}$) was used by Lu *et al.* [6] as a catalyst for hydrolysis of cellulose under mechano-chemical activation. Furthermore, Chen *et al.* [2] used $Cr(NO_3)_3$ as a hydrolyzing agent, while TEMPO-mediated oxidation of NCCs in alkaline conditions was applied by Sadeghifar *et al.* [5].

Beck-Candanedo *et al.* [7] indicated that the hydrolysis duration is one of the most important parameters affecting the hydrolysis products of wood pulp. The effect of the reaction conditions on NCCs-surficial charge and sulfur content was not significant and was controlled by factors other than hydrolysis conditions. However, chiral nematic pitch decreases when increasing the cellulose concentration and decreasing the NCCs length. Accordingly, aspect ratio of the NCCs also affects their chiral nematic property.

Araki *et al.* [4] found that H_2SO_4 provided more stable aqueous suspensions of NCCs than did HCl. The NCCs produced by HCl had minimum surficial charge, while those synthesized by H_2SO_4 were found to have a negatively charged surface [8]. This is due to the esterification process occurred for their surficial hydroxyl groups to give charged sulfate groups [7].

In addition, Bondeson *et al.* [9] emphasized the importance of duration and temperature of hydrolysis together with the H_2SO_4 concentration as important singular factors in the process of preparation of negatively charged isolated cellulose whiskers in water. Cellulose whiskers with a length ranging between 200 and 400 nm were obtained by using H_2SO_4 (63.5 wt/wt %) for approximately two h and with a yield of 30%.

An efficient green high-yield approach was applied by Lu *et al.*, [6] to produce high yield of NCCs (up to 88.4%) using $H_3PW_{12}O_{40}$-catalyst through a mechano-chemical hydrolysis.

Crystallographic scientists have controlled several properties of the NCCs such as composition, size, shape, structure and surficial properties [10]. Geometrical characteristics such as size, dimensions and shape of NCCs depend on the nature of the cellulose source as well as the hydrolysis conditions such as duration, temperature, ultrasonic treatment, and purity of materials [7,11,12]. Above a critical concentration point, the rod-like shape of

the charged NCCs leads to the formation of an anisotropic liquid crystalline phase [7,13]. Nevertheless, typical dimensions of whiskers range from 5 to 10 nm in diameter and from 100 to 500 nm in length.

In a stable cellulose nanofibrils (CNF) suspension, the distances among fibrils are not small enough to form molecular contact. Upon drying, forces resulting from the removal of water and high temperatures may drive the molecular contact of the CNFs and subsequently cause agglomeration. There are four methods can be performed to dry the NCCs, namely freeze drying, spray-drying, oven drying and supercritical drying [14].

There are several methods for calculating CI from XRD data, including the peak height method (PHM), Jayme-Knolle method (JKM), and modified Ruland-Vonk method (MRVM). Furthermore, Smoothing and differentiation are necessary in the XRD analysis to separate the true effects of the X-ray on a material's molecules [15,16]. Materials with high crystalline cellulose content (with high CI) give a sharp peak with a high intensity, whereas those with large amounts of amorphous components such as lignin, hemicelluloses, pectin, and amorphous cellulose (with low CI) give a broad peak with a low intensity [17,18]. The crystallographic characteristics can be investigated by various techniques and computation methods using XRD, ^{13}C-nuclear magnetic resonance (^{13}C-NMR), Fourier transform infrared (FTIR), and Raman spectroscopies [19,20,21].

The CI of cellulose is differed according to the cellulosic precursor, smoothing algorithms used for handling the XRD data, calculation methods and measurement technique used [15,19,20,22]. It was found by Hindi [23] that the XRD-diffractograms of two seed flosses (*Ceiba pentandra* and *Calotropis procera*) had a broad peak at 2θ of 18° for amorphous components and a sharp peak at approximately 22° related to crystalline components. Furthermore, the CI of seed floss of *Calotropis procera* was 65.5%, which approaches that for wood pine (70%) indicated by Borysiak and Doczekalska [24] and lies within the CI range (41.5% to 95.5%) shown by Park *et al*. [2010], (56% to 78%) by Terinte *et al*. [20], 79.6% obtained by Lu et al., [6] and 86.5% found by Chen *et al*. [2] for different cellulosic precursors using different measuring techniques. The higher crystallinity investigated by the wide angle-XRD for *Calotropis procera* seed floss than that for *Ceiba pentandra* reflects lower amorphicity for the former resource in its fiber wall nanostructure, which offers an additional mechanism for the latter to sorb more fluids [25]. The CI of Avicel cellulose differed significantly, from 39% to 67% according to the measurement technique used [22]. The ranges of the reported CI were 56% to 78%, 65% to 83%, and 37% to 93% for cotton linters, microcrystalline cellulose, and Avicel PH – 101, respectively [20].

Lu *et al*., [6] produced NCCs with higher thermal stability by combining mechanochemical activation and phosphotungstic acid hydrolysis. It was emphasized by Chen et al., [2] that better thermal stability of NCCs synthesized by $Cr(NO_3)_3$ (344°C) compared to those produced by H_2SO_4 (273°C) will force the former material to be regarded as a high potential filler for industrial nanocomposite applications.

It was reported by Dufresne [11] that neutralization of cellulosic nanoparticles, synthesized by sulphuric acid, by using NaOH can enhance their thermal stability.

2. Materials and Methods

The study was performed during 2015-2016 in the Central Laboratory at the Agricultural Research Station (ARS), Hada Al-Sham, King Abdul-Aziz University, about 120 km northeastern of Jeddah.

2.1. Raw Material

Woody branches of *Zizyphus spina* var christi (L.) Desf. was chosen for cellulosic fibers maceration and subsequent NCCs-production. Four healthy Zizyphus shrubs of 12 years old-stand were chosen randomly and three branches of each tree were selected. The branches were pruned in April by cutting at 5 cm above their branching level and specified for the maceration process. The mean diameter outside bark varied from 5 to12 cm.

Figure 1. *Zizyphus spina Christi*: a) the branches precursor for cellulose isolation, and b) the hydrolysis apparatus used for nanocrystalline cellulose synthesis

2.2. Samples Preparation

From each of the selected branches, one disc (about 20 cm along its grain) was removed at about 10 cm above the branching level. After excluding the pith and bark, the remainder wood of the disc was cross-cut into cubes (2 cm long each), Then, wood cubes were converted into thin chips (2 cm×2 cm×1 mm thick). The wood samples were extracted through a tertiary stage by a mixture (1:2) of ethyl alcohol (95 %)-benzene, ethyl alcohol (95 %), and finally by hot water for three hours in a Soxhlet apparatus according to ASTM [26] and Hindi *et al*. [27].

Five grams of thin chips from each of the three branches of each tree were digested separately using the Franklin method using a mixture of hydrogen peroxide (35%) and glacial acetic acid in a ratio of 1: 1, and kept at 60°C until the clear whiteness aspect. The oven-dried macerated fibers were used as a precursor for the NCCs synthesis.

2.3. Synthesis of NCCs

The NCCs were synthesized from the macerated cellulosic fibers by H_2SO_4, 64 % w/w [3] at 70°C with continuous stirring for an hour. The reaction was quenched by diluting the solution up to 20 fold by deionized water. The suspension was centrifuged at 1500 rpm to remove unhydrolyzed fibers and then at 14000 rpm for 20 min to obtain the NCCs. The precipitate was collected, re-centrifuged, and dialyzed against deionized water until neutralization. No sonication exposure was done upon the NCCs synthesis.

2.4. NCCs Characterization

The studied traits for the oven-dried NCCs particles were length and width that were used to calculate their aspect ratio. Moreover, the crystallinity index (CI), crystallite size (CS) and lattice spacing (LS) by XRD, mass loss by thermogravimetric analysis (TGA), and the difference in the sample's enthalpy (as exothermic or endothermic reactions) via differential thermal analysis (DTA) were applied to characterize the NCCs properties.

2.4.1. Optical Microscopy

An optical speculation unit consisted of a light microscope (CE- MC200A) in a magnification power of 10X with suitable vision system (OPTIKA PRO 5 Digital Camera- 4083.12, OPTIKA, Italy) with a Vision PRO 4 software was used to pick up, processing images, record different measurements of the NCCs-needles and monitoring their crystal growth [3,28].

One drop of recently prepared nanometric NCCs supernant, immediately at the end of the hydrolysis duration, was mounted and spread onto a glass slide without staining. One slide was specified to represent each of the four replicates of the wood species. The aspect ratio (length/width) of the NCCs-needles was calculated. About twenty needles were observed from each slide.

2.4.2. Scanning Electron Microscopy (SEM)

The oven-dried NCCs powder was redissolved in deionized water and sonicated using a digital ultrasonic Cleaner HB-4818 T. One drop of the previously filtered NCCs supernant was mounted and spread onto a double side carbon tape on Al-stub and dried. Before testing, the samples were sputtered with a 15 nm thick gold layer (JEOL JFC- 1600 Auto Fine Coater) in a vacuum chamber [29]. The samples were examined with a SEM Quanta FEG 450, FEI, Amsterdam, Netherland at an accelerating voltage differing between 5-20 kV. The length and width of the oven-dried NCCs particles were measured and the aspect ratio of them were calculated.

2.4.3. X-Ray Diffraction (XRD)

The wide-angle XRD spectra of the oven-dried NCCs particles were obtained using an XRD 7000 Shimadzu diffractometer, Japan [15]. For the XRD system, CuKα radiation was consisted of Kα1 (0.15406 nm) and Kα2 (0.15444 nm) and was induced at 30 kV and 30 mA. The CuKα radiation was extracted from the data using a single-channel analyzer. Each divergence and scatter slits was 1°, and the receiving slit was 0.15 mm at the same radius. Oven-dried NCCs samples (about 0.5 g) were mounted onto quartz using a dry amorphous glue. The two theta angle range of 10°-30° was used to study the crystallographic properties of the NCCs. All runs were operated in the reflection mode with scanning velocity of 4°/min in 0.05°-steps.

When the cellulosic sample was X-rayed, a stream of crude data representing x- and y-coordinates (2θ and I, respectively) of all points representing the XRD diffractometer was obtained (Figure 4). The XRD data were processed using curve table-software for smoothed data fitted by the Savitzky-Golay algorithm.

2.4.3.1. Crystallinity Index (CI)

After the individual crystalline peaks were smoothed, the CI was calculated as a percentage of the crystalline diffractogram area based on the original diffractogram area using the following equation [15]:

$$CI = \left[\left(D_{cr1} + D_{cr2} \right) / D_t \right] X100$$

where D_{cr1} is the area under the 1st crystalline peak representing the 110 and $11\bar{0}$ planes together, D_{cr2} is the area under the 2nd crystalline peak related to the 200 crystallographic plane, and the D_t is the area under the total diffractogram.

2.4.3.2. Crystallite size (CS)

The CS was calculated by the Scherrer equation [30,31] as follows:

$$CS = \left(57.3k\lambda \right) / \left(\beta \cos\theta \right)$$

where CS is the average diameter of the crystallite, k is the form factor of the crystallite (0.94), λ is known to be wavelength of X-ray accident to the crystallite (0.1542 nm), β is the full width at half maximum (FWHM) of the crystalline peak represented to the crystallographic plane 200, and θ is the Bragg's angle related to the 002-plane. A factor of 57.3 is multiplied by kλ to convert β from degrees to radians in the above mentioned equation.

2.4.3.3. Lattice Spacing (*d*)

The *d* value was calculated using the Bragg's equation mentioned below:

$$d = n\lambda / 2\sin\theta$$

where n is an ordinal number taking a value of "1" for diffractograms having the strongest intensity [66], λ is the wavelength of X-rays incident on the crystal (0.1542 nm), and θ is the Bragg's angle corresponding to the 200-plane [15].

2.4.4. Thermal Analysis

Analyzing the thermal properties of the NCCs is important to monitor their processing temperature range and utilization. In the present investigation, the thermal analysis was restricted to two characterization for the resulted NCCs, namely thermogravimetric analysis (TGA) and differential thermal analysis (DTA) using a Seiko & star 6300 analyzer, Central Laboratory, Faculty of Science, Alexandria University, Egypt. Heating was scanned from 30°C up to 500 °C with an increasing rate of 20 °C/min in a flowing nitrogen atmosphere [3,32].

The mass loss of the NCC was calculated from the TGA curve presented in Figure 5 using the following equation:

Mass loss=$[(W_2-W_1)/W_1]\times 100$, where

W_1= Initial NCCs weight for such a temperature region.

W_2= Final NCCs weight for the same temperature region.

2.5. Statistical Design and Analysis

Completely randomized block design with four replications was performed in this study using the analysis of variance method. Furthermore, the differences between means were examined using the least significant difference test (LSD) at P≤0.05 according to Steel and Torrie [33].

2.6. Objectives

The target of this work is to evaluate the quality properties of the nanocrystalline cellulose (NCCs) synthesized from cellulosic fiber macerated from *Zizyphus spina christi* wood.

3. Results and discussion

3.1. Optical Microscopy (OM)

The OM findings indicated some dimensional insights corresponding to the needles architectures constructed upon crystal growth of the nanometric-scaled NCCs-acidic solution. This growth from nano- into micrometric scale showed the ability of the NCCs for self-organization or so-called self-assembly. It was noticed that after about 30 minutes after spreading a drop of the hydrolysis supernant, immediately after completing the hydrolysis process, onto a glass substrate, the NCCs spherulites were agglomerated into bigger aggregates belongs to colloidal state which in turn were aligned straightly to form needle-shaped architectures. The driving force for this crystal growth process can be restricted to the following effects: a) electrostatic forces on the NCCs surfaces due to the grafted functional groups (protons, sulfate and hydroxyl), b) the H_2SO_4-concentration gradient, and c) the difference between surface tensions of solution, air and glass. The net force generated at this interface is considered as the driving force of the NCCs-crystal growth process. Accordingly, the needles were imagined to be formed by electrostatically end to end attraction and subsequent self-welding (Figure 2).

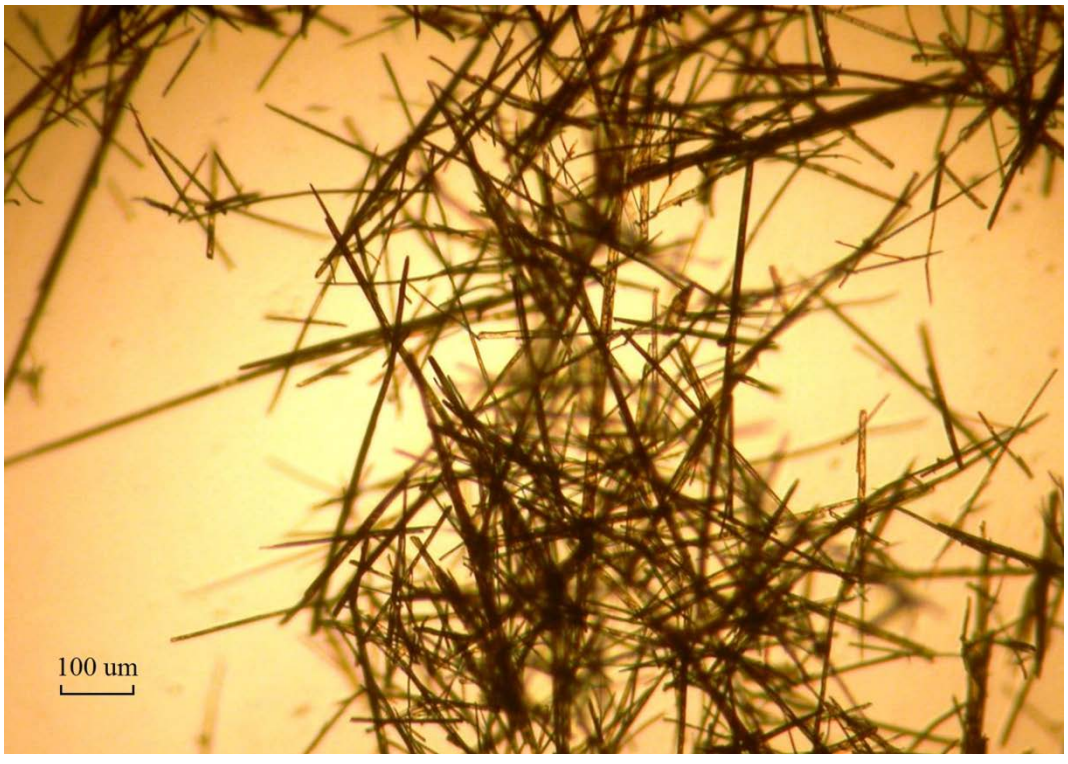

Figure 2. An optical image of the needle-shaped nanocrystalline cellulose (NCCs) of *Zizyphus spina christi* directly in an acidic media on a glass substrate

3.2. Scanning Electron Microscopy (SEM)

The SEM micrograph of the NCCs particles is presented in Figure 3. It is clear that the NCCs are finally aggregated, after oven-drying, in a short rod-shaped with a vast range of particle size distribution. The final rod lengths varied from 1.875 µm to 26.25 µm, while their widths ranged from 0.75 µm to 5.25 µm.

3.3. Aspect Ratio of the NCCs Needles and Powder

The aspect ratio of the NCCs-Needles was ranged from 50 to 100 based on the optical microscopy speculation (Figure 2). For the aspect ratio of the oven-dried NCCs particles based on the SEM study, it was calculated to be 2.5-5. The aspect ratio of the NCCs-needles was about 20 times higher than that for the NCCs-powder. The high aspect ratio of the NCCs-needles add a valuable feature for them, but unfortunately, this architecture is unstable and are fractured into short rods with the evaporation of the acidic media or under neutralization and filtration process.

For the aspect ratio of the oven-dried NCCs particles, it was smaller than many literatures such as those found by Tonoli *et al*. [34] for micro/nanofibrils (10-50), and Sacui, *et al*. [35] for NCCs (23±12-148±147). Since colloidal NCCs rods having high aspect ratio have been getting wide acceptance in the global markets due to their exquisite mechanical properties, chirality, sustainability, and availability [1], the oven-dried NCCs must be converted into nanocolloidal form to be included in a composite material to enhance their aspect ratio.

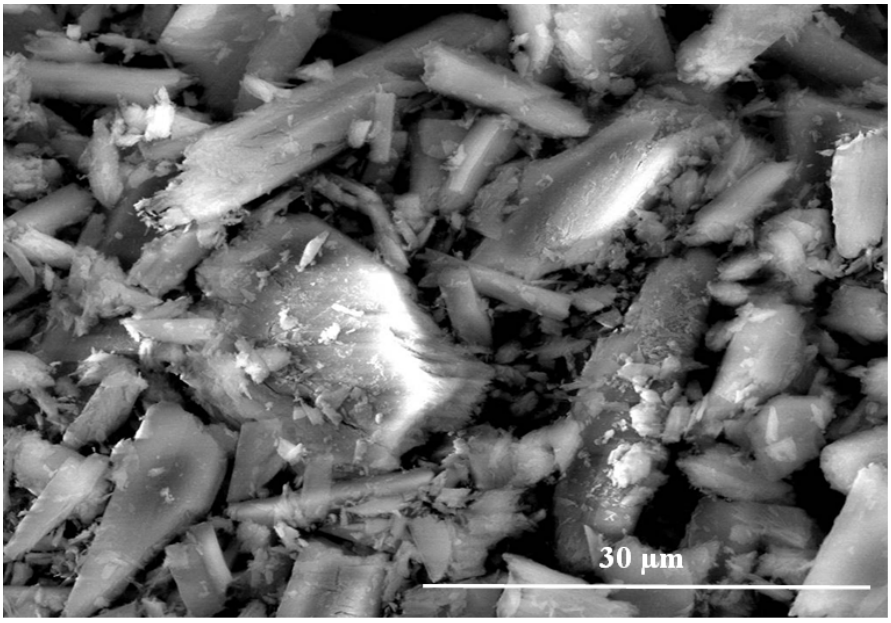

Figure 3. SEM micrograph of agglomerated particles of nanocrystalline cellulose (NCCs) of *Zizyphus spina christi* after oven drying

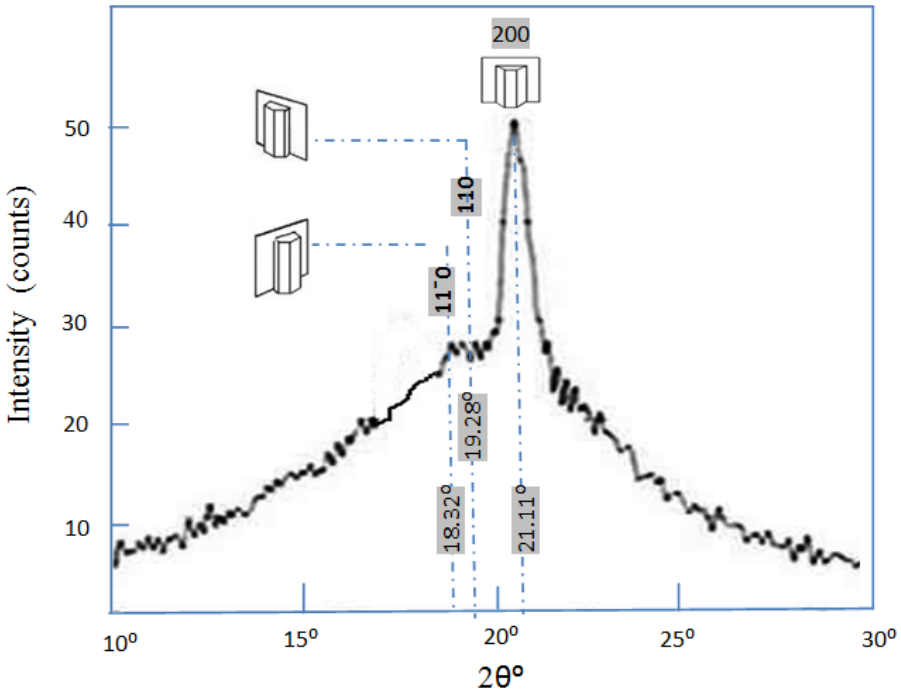

Figure 4. X-ray diffractogram (XRD) of nanocrystalline cellulose (NCCs) of *Zizyphus spina christi*

3.4. X-Ray Diffraction (XRD)

The NCCs samples exhibited a principle sharp peak around $2\theta = 21.11^{o}$ representing the 200 reflection related to hemicelluloses and alpha-cellulose (Figure 4).

In addition, the NCCs sample showed two broad peaks at $2\theta = 18.32^{o}$ and 19.28^{o} representing 110 and $1\bar{1}0$ reflections. Accordingly, the similarity between the resultant NCCs and cellulose-I was clear, especially when regarding the crystallographic planes, namely 110, $1\bar{1}0$ and 200 [36,37,38] as indicated in Figure 4.

3.4.1. Crystallinity Index (CI)

The CI of the NCCs was found to be high (86.75%) indicating that the CI of this material was increased after removing the amorphous component via acid-hydrolysis. The obtained CI was higher than those obtained for cellulose and NCCs (70.62 and 76.01%, respectively) that found by Wulandari *et al.* [39], seed floss of *Calotropis procera* (65.5%) [23], wood pine (70%) that indicated by Borysiak and Doczekalska [24], 79.6% that obtained by Lu *et al.* [6], and lies within the CI ranges (41.5% to 95.5%) that shown by Park *et al.* [19], and (56% to 78%) determined by Terinte *et al.* [20], and approaches to the 86.5% value found by Chen *et al.* [2] for different cellulosic precursors using different measuring techniques.

3.4.2. Crystallite Size (CS)

The crystallite size (CS) is the crystallite thickness estimated by the Scherrer formula for the crystallites having a size less than 100 nm [30]. The average CS of the NCCs was measured to be 2.78 nm that is similar to that found by Hindi [3], and smaller than that for cellulose I (about 5 nm in width). The CS finding is in agreement with the data range found by Hindi [15]. It is worth mentioning that, XRD resolution is not adequate for small crystallites to obtain accurate imagination concerning their lattice structure [40].

3.4.3. Lattice Spacing (LS)

The LS of the NCCs is a measure of the distance between their successive cellulosic strata within a crystallite [40]. Using the Bragg's equation, the distance between the strata was found to be 0.214 nm. Since larger crystal size leads to larger LS between its crystalline strata [41], the lower LS value can be attributed to the small size of the NCCs crystallite estimated in the present study (2.78 nm). The LS result is slightly smaller than that found by Hindi [15].

3.5. Thermal Analysis

3.5.1. Thermogravimetric Analysis (TGA)

The TGA thermogram (Figure 5) clearly indicates a gradual increase in losing weight of the NCCs upon heating them from 25°C up to 500°C in an inert atmosphere of a flowing N_2-gas. The entire heat range was divided into five individual regimes, namely 25-100°C, 100°C-200°C, 200°C-300°C, 300°C-400°C, and 400°C-500°C to study the mass loss of the NCCs occurred at each regime. The primary mass loss for the NCCs was 5.26 % as temperature increased from 25°C to 100°C due to elimination of free water [3]. In addition, the NCCs have lost about 22.3 % of their mass when the temperature was raised from 100 up to 200°C due to evaporation of both hygroscopic and constitutional water. Between 200°C-300°C, the NCCs mass loss was lower than that recorded for the 2nd thermal degradation regime (12.24 %). Afterward, the NNCs was continued to lose part of their mass as 25% and 16.7 % for the 4th (300°C-400°C) and 5th (400°C-500°C) regimes, respectively**.** It can be seen from Figures 5 and 6 that the mass loss was shifted at the 2nd and the 4th regimes comparing to the other thermal degradation regimes. At lower temperatures, the thermal degradation of the sulphated NCCs can be attributed to presence of huge free ends in chains of the highly sulfated regions (HSR). It worth mentioning that the HSR have less crystalline nature that makes them more susceptible to thermal elimination [42] as volatile byproducts and may lead to drastic reduction in the NCC-molecular weight. In addition, elimination of the sulphate groups in sulfated anhydro-glucose units require less energy [43], therefore, sulfuric acid molecules were arisen at lower temperatures upon the thermal degradation process.

On the other hand, the low thermal stability of the sulphated NCCs at higher temperatures can be related to the degradation of unsulphated components of the NCCs material [44].

3.5.2. Differential Thermal Analysis (DTA)

DTA is a measure tool to differentiate two hot materials, the 1st one is the NCCs and the 2nd one is an inert reference material. Both materials are found at the same place and conditions. As shown in Figure 7, there is an endothermic peak (under the baseline) as well as one exothermic peak (above this line). The endothermic peak starts from 39°C up to 277°C with a maximum value at 150°C, while the exothermic peak begins from 277°C until 460°C with a maximum shift at 356°C (Figure 7 and Table 1).

The endotherm of the DTA results can be attributed to evaporation of the three forms of moisture content in the NCCs, namely free, hygroscopic and constitutional moisture along with fusion or melting process of the NCCs. Furthermore, losing moisture is companied to this endotherm at higher temperatures [36]. The evaporation process depends essentially on the difference in holding capacity of moisture by the sorptive forces [36] arisen between water molecules and the NCCs-crystallites. For the sulphated NCCs, the hydrolyzing agent used in this study (H_2SO_4) acted as a dehydrating agent and helped for grafting the sulphate groups which are well-known by their hydrophobicity that lowering the NCCs-affinity for moisture sorption. It worth to mention that after hydrolysis of the macerated cellulosic fibers, all amorphous regions were dissolved and only nano-scale cellulose crystals would possess sulphate groups that responsible for the higher onset temperature of crystal melting with wider endotherm width.

The exotherm occurred between 277°C and 500°C can be attributed to depolymerization of the sulphated NCCs, decomposition of glycosyl-units and then formation of a carbonaceous residues (36). This depolymerization can be illustrated by four reasons: a) due to nano-size and greater number of the free ends of the chains of NCCs which

decompose at a lower temperature, b) H_2SO_4 (a dehydrating agent) which facilitate the depolymerization of cellulose by removing some hydroxyl groups [45], c) the presence of H^+ ion in the weak acidic atmosphere (pH 5.5-6) that increased the char residues because of removal of oxygen in the form of H_2O which prevent weight losses, and (d) the highly crystalline nature of CNCs increased the carbon residues [38,45].

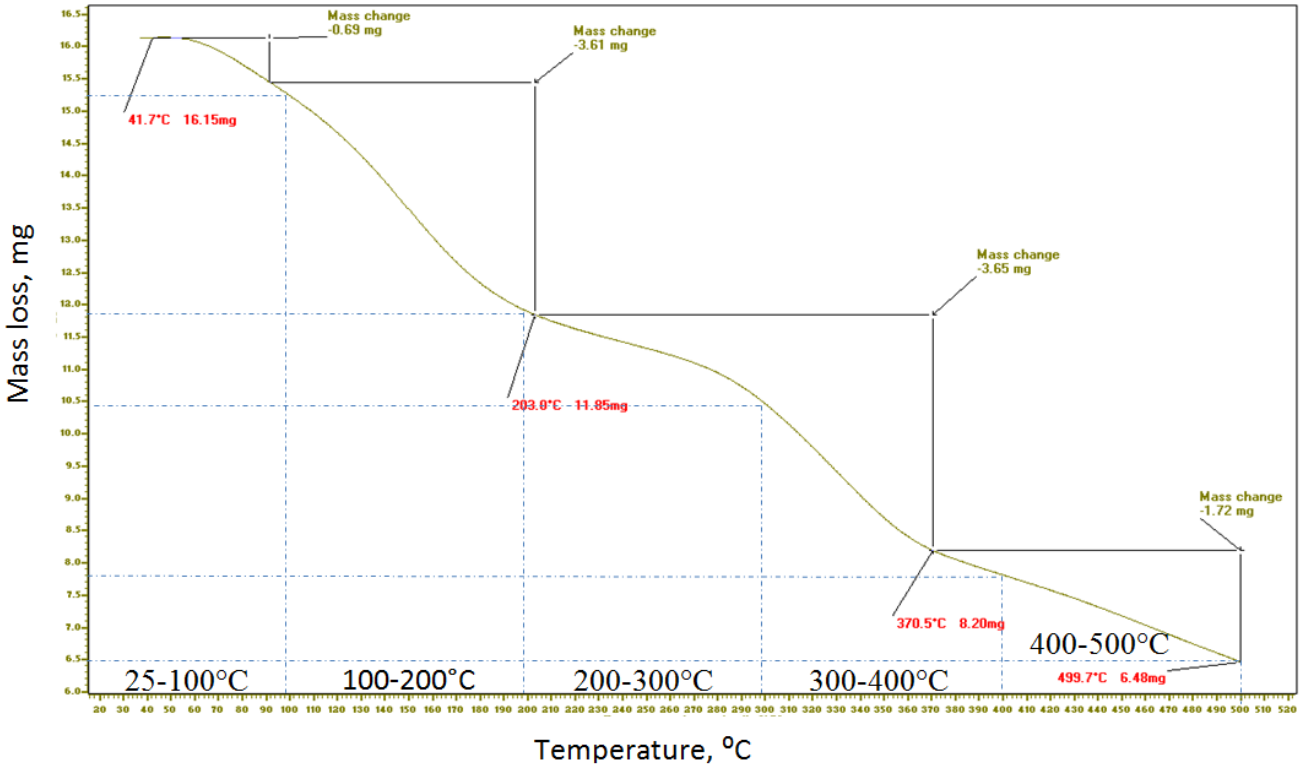

Figure 5. Thermogravimetric analysis (TGA) of the nanocrystalline cellulose (NCCs)

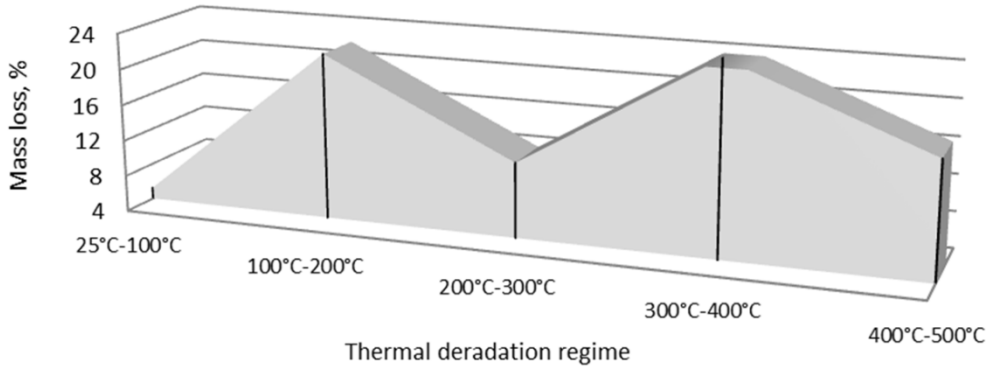

Figure 6. Thermogravimetric analysis (TGA) of the nanocrystalline cellulose (NCCs)

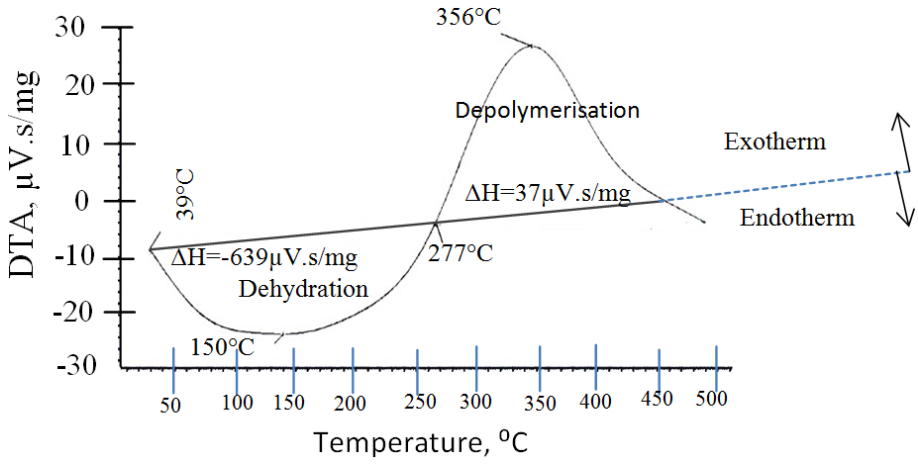

Figure 7. Differential thermal analysis (DTA) of nanocrystalline cellulose (NCCs) of *Zizyphus spina christi*

Table 1. Differential thermal analysis (DTA) data for temperature region (TR), maximum temperature shift (MTS) and enthalpy change (EG) of the nanocrystalline cellulose (NCCs) upon thermal exposure up to 500°C

Thermogram		TR (°C)	MTS (°C)	EG (µVs/mg)
No	type			
1	Endotherm	39-277	149.6	-639
2	Exotherm	277-460	355.3	37

Furthermore, the absolute value of the heat change values for the endotherms was 639 µVs/mg that is extremely higher than that released due to the exotherm (37 µVs/mg). Since the material absorbing higher energy are more thermally stable than those absorbing lower energy or releasing more energy upon exothermic reactions [32], the NCCs have a good thermal stability behavior.

4. Conclusion

- Crystal growth of the nanocrystalline cellulose from nano-into more organized-micrometric-scaled architectures confirmed their ability to self-assembly.
- The nanocrystalline cellulose spherulites were agglomerated into bigger aggregates upon crystal growth on a glass substrate in an acidic media.
- The driving forces for the crystal growth process are electrostatic forces on the crystallite surfaces, the H_2SO_4-concentration gradient, and the difference between surface tensions of solution, air and glass.
- The nanocrystalline cellulose diffractogram was similar to that known for cellulose I.
- The crystallinity index of the nanocrystalline cellulose was higher than that for cellulose I confirming elimination of amorphous components due to acid-hydrolysis.
- The thermogravimetric analysis indicated a gradual increase in their mass loss of the synthesized NCCs upon heating them from 25°C up to 500°C in a flowing N_2-atmosphere.
- Differential thermal analysis showed the presence of an endothermic peak (due to evaporation) and one exothermic peak (due to depolymerization and decomposition of the nanocrystalline cellulose
- Based on the results, the Zizyphus wood is suitable precursor for nanocrystalline cellulose production.

Acknowledgments

This project was funded by the Deanship of Scientific Research (DSR), King Abdulaziz University, Jeddah under grant no. 115/155/1432. The author therefore, acknowledges with thanks DSR technical and financial support.

References

[1] Majoinen, J., Kontturi, E., Ikkala, O., and Gray, D. G. 2012. SEM imaging of chiral nematic films cast from cellulose nanocrystal suspension. Cellulose, 19: 1599.

[2] Chen, Y. W., Tan, T. H., Lee, H. V., and Abd Hamid, S. B. 2017. Easy fabrication of highly thermal-stable cellulose nanocrystals using $Cr(NO_3)_3$ catalytic hydrolysis system: A feasibility study from macro- to nano-dimensions. Materials, 10: 42.

[3] Hindi, S. S, Z. 2017[a]. Suitability of date palm leaflets for sulphated cellulose nanocrystals synthesis. Nanoscience and Nanotechnology Research. 4 (1): 7-16.

[4] Araki, J., Wada, M. Kuga, S., and Okano, T. 1998. Low properties of microcrystalline cellulose suspension prepared by acid treatment of native cellulose. Colloids Surf. *A*, 142: 75-82.

[5] Sadeghifar, H. , Filpponen, I., Clarke, S. P., Brougham, D. F., and Argyropoulos, D. S. 2011. Production of cellulose nanocrystals using hydrobromic acid and click reactions on their surface J Mater Sci. 46: 7344.

[6] Lu, Q., Cai, Z., Lin, F., Tang, L., Wang, S., and Huang, B. 2016. Extraction of cellulose nanocrystals with a high yield of 88% by simultaneous mechanochemical activation and phosphotungstic acid hydrolysis. ACS Sustainable Chem. Eng., 4 (4): 2165-2172.

[7] Beck-Candanedo, S., Roman, M., and Gray, D. G. 2005. Effect of reaction conditions on the properties and behavior of wood cellulose nanocrystal. Biomacromolecules, 6 (2): 1048-54.

[8] Dufresne, A. 2012. Nanocellulose: From nature to high performance tailored materials. Walter de Gruyter GmbH & Co. KG: 475 pp.

[9] Bondeson, D., Mathew, A. and Oksman, K. 2006. Optimization of the isolation of nanocrystals from microcrystalline cellulose by acid hydrolysis. Cellulose, 13: 171-180.

[10] Yin, Y. and Alivisatos, A. P. 2005. Colloidal nanocrystal synthesis and the organic-inorganic interface. Nature, 437: 664-670.

[11] Dufresne, A. 2013. Nanocellulose: a new ageless bionanomaterial. Materialstoday, 16 (6): 220-227.

[12] Azizi Samir, M. A. S., Alloin, F. and Dufresne, A. 2005. Review of recent research into cellulosic whiskers, their properties and their application in nanocomposite field. Biomacromolecules, 6: 612-626.

[13] Dong, X. M., Revol, J. F., Gray, D. 1998. Effect of microcrystallite preparation conditions on the formation of colloid crystals of cellulose. Cellulose, 5: 19-32.

[14] Pakowski, Z. 2007. Modern methods of drying nanomaterials. Transp. Porous Med., 66:19-27.

[15] Hindi, S. S. Z. 2017[b]. Some crystallographic properties of cellulose I as affected by cellulosic resource, smoothing, and computation methods. International Journal of Innovative Research in Science, Engineering and Technology, 6 (1): 732-752.

[16] Luo, J., Ying, K., and Bai, J. 2005. Savitzky-Golay smoothing and differentiation filter for even number data. Signal Processing, 85 (7): 1429-1434.

[17] Mwaikambo, L.Y., and Ansell, M. P. 2002. Chemical modification of hemp, sisal, and kapok fibers by alkalization, Journal of Applied Polymer Science, 84 (12): 2222-2234.

[18] Jayaramudu, J., Guduri, B. R., and Rajulu, A. V. 2010. Characterization of new natural cellulosic fabric *Grewia tilifolia*, Carbohydrate Polymers, 79 (4): 847-851.

[19] Park, S., Baker, J. O., El-Himmell, M., Parilla, P. A., and Johnson, D. K., 2010. Cellulose crystallinity index: Measurement techniques and their impact on interpreting cellulase performance. Biotechnology for Biofuels, 3: 10.

[20] Terinte, N., Ibbett, R., and Schuster, K. C. 2011. Overview on native cellulose and microcrystalline cellulose I structure studied by X-ray diffraction (WAXD): Comparison between measurement techniques. Lenzinger Berichte, 89: 118-131.

[21] Schenzel, K., Fischer, S., and Brendler, E. 2005. New method for determining the degree of cellulose I crystallinity by mean of FT Raman spectroscopy. Cellulose, 12 (3): 223-231.

[22] Thygesen, A., Oddershede, J., Lilholt, H., Thomsen, A. B., and Stahl, K. 2005. On the determination of crystallinity and cellulose content in plant fibers. Cellulose, 12 (6): 563-576.

[23] Hindi, S. S. Z. 2013[a]. *Calotropis procera*: The miracle shrub in the Arabian Peninsula. International Journal of Science and Engineering Investigations, 2 (16): 10 pp.

[24] Borysiak, S. and Doczekalska, B. 2005. X-ray diffraction study of pine wood treated with NaOH. Fibers and Textiles in Eastern Europe, 5 (53): 87-89.

[25] Hindi, S. S. Z. 2013[b]. Characteristics of some natural fibrous assemblies for efficient oil spill cleanup. International Journal of Science and Engineering Investigations, 2 (16): 10 pp.

[26] ASTM D1105-84, Standard method for preparation of extractive-free wood, ASTM International, West Conshohocken, PA, 1989.

[27] Hindi, S. S. Z., A. A. Bakhashwain and A. A. El-Feel. 2011. Physico-chemical characterization of some Saudi lignocellulosic natural resources and their suitability for fiber production. JKAU; Met. Env. Arid Land Agric. Sci., 21 (2): 45-55.

[28] Hindi, S. S. Z. and Abohassan, R. A. 2015. Cellulose triacetate synthesis from cellulosic wastes by heterogeneous reactions. Bioresources, 10 (3), 5030-5048.

[29] Tang, L. G., Hon, D. N. S., and Zhu, Y. Q. 1997. An investigation in solution acetylation of cellulose by microscopic techniques. Journal of Applied Polymer Science, 64 (10): 1953-1960.

[30] Ciupina, V., Zamfirescu, S., and Prodan, G. 2007. Evaluation of mean diameter values using Scherrer equation applied to electron diffraction images, In: Nanotechnology-Toxicological Issues and Environmental Safety, NATO Science for Peace and Security Series: 231-237.

[31] Poletto, M., Ornaghi, H. L. and Zattera, A. J. 2014. Native cellulose: Structure, characterization and thermal properties. Materials, 7 (9): 6105-6119.

[32] Sherif S. Hindi, Mona O. Albureikan , Attieh A. Al-ghamdy, Haya Alhummiany and M. Shahnawaze Ansari. 2017. Synthesis and characterization of gum Arabic based bio-plastic membranes. Nanoscience and Nanotechnology Research, 4 (1): 32-42.

[33] Steel, R. G. D. and Torrie, T. H. 1980. Principles and procedures of statistics, N. Y., USA.

[34] Tonoli, G. H. D., Teixeira, E. M., Corrêa, A. C., Marconcini, J. M., Caixeta, L. A., Pereira-da-Silva, M. A., and Mattoso, L. H. C. 2012. Cellulose micro/nanofibres from *Eucalyptus* kraft pulp: Preparation and properties. Carbohydrate Polymers, 89 (1,5): 80-88.

[35] Sacui, I. A. *et al*., 2014. Comparison of the Properties of cellulose nanocrystals and cellulose nanofibrils isolated from bacteria, tunicate, and wood processed using acid, enzymatic, mechanical, and oxidative methods. ACS Appl. Mater. Interfaces, 6 (9): 6127-6138.

[36] Kumar, A., Negi, Y. S., Choudhary, V. and Bhardwaj, N. K. 2014. Characterization of cellulose nanocrystals produced by acid-hydrolysis from sugarcane bagasse as agro-waste. Journal of Materials Physics and Chemistry, 2 (1): 1-8.

[37] Chen, W. S., Yu, H. P., Liu, Y. X., Chen, P., Zhang, M. X., and Hai, Y. F. 2011. Individualization of cellulose nanofibres from wood using high-intensity ultrasonication combined with chemical pretreatments. Carbohydr. Polym., 83: 1804-1811.

[38] Wada, M., Heux, L., and Sugiyama, J. 2004. Polymorphism of cellulose I family: Reinvestigation of cellulose IV. Biomacromolecules, 5: 1385-1391.

[39] Wulandari, W. T., Rochliadi, A., and Arcana, I. M. 2016**.** Nanocellulose prepared by acid hydrolysis of isolated cellulose from sugarcane bagasse. IOP Conf. Series. Materials Science and Engineering, 107: 012045.

[40] Clair, B., Almeras, T., Yamamoto, H., and Okuyama, J. 2006. Mechanical behavior of cellulose microfibrils in tension wood, in relation with maturation stress generation. Biophysics Journal, 91 (3): 1128-1137.

[41] Davidson, T., Newman, R. H., and Ryan, M. J. 2004. Variations in the fibre repeat between samples of cellulose I from different sources. Carbohydrate Research, 339 (18), 2889-2893.

[42] Mandal, A., and Chakrabarty, D. 2011. Isolation of nanocellulose from waste sugarcane bagasse (SCB) and its characterization. Carbohydr. Polym., 86: 1291-1299.

[43] Julien, S., Chomet, E., and Overend, R. P. 1993. Influence of acid pre-treatment (H_2SO_4, HCl, HNO_3) on reaction selectivity in the vacuum pyrolysis of cellulose. Journal of Analytical and Applied Pyrolysis, 27(1), 25-43.

[44] Maren, R., and William, T. W. 2004. Effect of sulfate groups from sulfuric acid hydrolysis on the thermal degradation behavior of bacterial cellulose. Biomacromolecules, 5: 1671-1677.

[45] George, J., Ramana, K. V., Bawa, A. S., and Siddaramaiah. 2011. Bacterial cellulose nanocrystals exhibiting high thermal stability and their polymer nanocomposites. Internl. J. Biologic. Macromol., 48: 50-57.